JPE 19-1-21

https://doi.org/10.6113/JPE.2019.19.1.220
ISSN(Print): 1598-2092 / ISSN(Online): 2093-4718

Design and Analysis of Universal Power Converter for Hybrid Solar and Thermoelectric Generators

Sathiyanathan M.†, Jaganathan S.*, and Josephine R. L.**

†Dept. of Electrical and Electronics Eng., PSG Institute of Technology and Applied Research, Coimbatore, India
*Dept. of Electrical and Electronics Eng., Dr. N.G.P. Institute of Technology, Coimbatore, India
**Dept. of Electrical and Electronics Eng., National Institute of Technology, Tiruchirappalli, India

Abstract

This work aims to study and analyze the various operating modes of universal power converter which is powered by solar and thermoelectric generators. The proposed converter is operated in a DC–DC (buck or boost mode) and DC–AC (single phase) inverter with high efficiency. DC power sources, such as solar photovoltaic (SPV) panels, thermoelectric generators (TEGs), and Li-ion battery, are selected as input to the proposed converter according to the nominal output voltage available/generated by these sources. The mode of selection and output power regulation are achieved via control of the metal-oxide semiconductor field-effect transistor (MOSFET) switches in the converter through the modified stepped perturb and observe (MSPO) algorithm. The MSPO duty cycle control algorithm effectively converts the unregulated DC power from the SPV/TEG into regulated DC for storing energy in a Li-ion battery or directly driving a DC load. In this work, the proposed power sources and converter are mathematically modelled using the Scilab-Xcos Simulink tool. The hardware prototype is designed for 200 W rating with a dsPIC30F4011 digital controller. The various output parameters, such as voltage ripple, current ripple, switching losses, and converter efficiency, are analyzed, and the proposed converter with a control circuit operates the converter closely at 97% efficiency.

Key words: DC–AC converter, DC–DC converter, Solar power generator, Thermoelectric generator, Universal power converter

I. INTRODUCTION

The rapid increase in energy requirements due to industrial growth, environmental issues, and fossil fuel depletion has increased the use of renewable energy sources for satisfying the power demand. Energy sources such as solar photovoltaic (SPV) generators, wind energy conversion (WEC) systems, thermoelectric generators (TEGs), and fuel cells (FCs) are currently used to harvest energy from energy storage systems (ESSs), such as battery banks, or directly connected to loads through power regulating devices. Among all renewable energy sources, solar and thermoelectric generators have received the most attention in electric power generation due to their availability. In [1], the International Energy Agency (IEA) stated that the power from SPV systems will satisfy approximately 45% of the energy needs of the world in the year 2040. SPV panels generate power on the basis of the sun's irradiation level and temperature. However, SPV systems fail to generate power under poor lighting and partial shading conditions. Thus, TEGs are considered an additional source of energy. TEGs deliver power according to the hot- and cold-side temperature difference on semiconductor surfaces. The inputs to these sources (irradiation and temperature) are reusable and non-pollutant but dynamic in nature. Another important aspect is the power transfer to remote areas, such as hill stations and forest areas that require long transmission lines, which have substantial line losses. A standalone hybrid power system is a suitable approach to efficient power transfer because individual power sources may fail to feed power to the load if the inputs to the sources are unavailable. In an SPV system, solar irradiation and temperature are absent during night hours. Similarly, the TEG module fails to generate power when the hot- and cold-side temperatures are absent. These individual sources require power electronic converters (PECs) for regulating input and output powers.

Manuscript received May 5, 2018; accepted Oct. 12, 2018
Recommended for publication by Associate Editor M. Vilathgamuwa.
†Corresponding Author: sathiyangm@gmail.com
Tel: +91-422-393-3666, Fax: +91-422-393-3456, PSG Institute of Technology and Applied Research
*Dept. of Electrical Eng., Dr. N.G.P. Institute of Technology, India
**Dept. of Electrical Eng., National Institute of Technology, India

In general, a standalone/hybrid renewable energy system uses different power converters, such as AC–DC/DC–DC/DC–AC controllers, which are controlled by individual digital controllers programmed with an intelligent control algorithm. In [2]-[4], and [5], the development of a buck converter with efficient control techniques for maintaining the highest efficiency was explained. In [6]-[8], and [9], a boost converter was designed for high-power applications while explaining the continuous conduction mode (CCM) and discontinuous conduction mode (DCM) of operations. A resonant boost converter was implemented for vehicle battery charging applications in [10] and analyzed for a wide range of load variations, with an efficiency of 97.4%. Similarly, a comparative study of boost converter design and performance parameters, such as power conversion efficiency, switching power losses, and voltage ripple, was conducted in [11]. Efficiency and other converter performance parameters of converters were ensured by pulse width modulation (PWM) signal generation to converter switches using intelligent control algorithms.

A control algorithm ensures the highest level of efficiency by operating the converter system at maximum power point (MPP) regardless of changes in external conditions. However, this arrangement creates complexity in control and increases the size and cost of the system. An MPP tracking controller typically consists of a step-up or step-down DC–DC converter, as explained in [12] and [13]. These converters are used to regulate the voltage and current at the load by using proper duty-cycle tuning circuit. Thus, conventional converters and control algorithms are not extremely effective in terms of voltage, current ripple reduction, and controller response for tracking the MPP of the system. The buck/boost converter can only provide support to driving DC loads. However, most appliances are manufactured to operate in AC voltage. Thus, the DC–AC power converter can convert fixed or variable DC into AC. A single-phase inverter was developed for low-power applications in [14] and [15], and PWM methods reduced the harmonic content [16] and maintained the highest level of power conversion efficiency. In [17]-[19], and [20], different inverter topologies were utilized for grid-connected and standalone PV applications and maintained the highest efficiency of 99.3%. Inefficient control algorithms and the use of individual power converters evidently lead to power loss and poor system efficiency. Hence, hybrid converter circuits were developed in [21]-[23], and [24]; they were operated in buck/boost mode with the highest efficiency.

However, additional advantages could be gained if the converters discussed above were implemented in a single converter topology called universal power converter (UPC). This converter is an extension of the DC–DC buck, boost converter, and inverter. Studies on this type of converter topology are limited. For example, a parallel AC-link universal power converter was proposed in [25] and used for DC–DC, DC–AC, AC–DC, and AC–AC conversions. However, the converter circuit uses numerous switches for the operation with soft-switching using a capacitor. A universal converter topology that is based on the buck-boost converter for energy harvesters in battery-powered applications was presented in [26]. This universal converter topology can be used as an AC–DC and DC–DC converter for energy harvesting in batteries and is unsuitable for DC–AC and AC–AC power conversion applications. In [27], an ultra-sparse AC-link buck-boost converter was proposed; it has a long life due to its soft-switching feature. However, this converter's performance also suffers due to the presence of many switching devices. In [28]-[30], only three-phase converters, with one- or two-power conversion operations, were discussed. These circuits also utilize many switches for power conversion.

From the above studies, a novel UPC is developed and presented in this research. The proposed converter can be operated in DC–DC, DC–AC, and AC–DC. The major advantages of the proposed UPC include simple structure, easy mode selection, and operation with only a few switches. Hence, the proposed converter achieves high efficiency in operation and low-cost construction. The modes of operation of the proposed converter in all configurations are explained in this paper. This converter is designed for energy harvesting from solar and thermoelectric generators in a battery bank and then feeding the power to DC/AC loads. Analysis is performed to improve the drawbacks of the power converter. Significant disadvantages include switching power loss and power quality issues, such as harmonics and efficiency.

The proposed UPC system is operated in three modes, and the performance of the converter is analyzed in individual modes. Mode-1 acts as a buck converter for storing energy in a Li-ion battery, Mode-2 acts as a boost converter for direct DC loads, and Mode-3 acts as a single-phase inverter for powering AC loads. Mixed-mode operation, that is, buck, boost, and inverter operation, is not implemented in this work. The paper is organized as follows. Section I describes various power converters and their design challenges. Section II presents the UPC design and analysis. Section III elaborates the control structure of the UPC. Section IV presents the simulation and hardware results. Finally, Section V concludes the paper with recommendations.

II. Analysis and Design of Universal Power Converter

The proposed UPC consists of nine MOSFET switches, two capacitors (one at the input and the other at the output), and a step-up transformer for effective operation, as illustrated in Fig. 1. Power sources, SPV, battery, TEG, and AC load can be selected by controlling switches Q_6, Q_7, Q_8, Q_5, and Q_9, respectively. Switches Q_1, Q_2, Q_3, and Q_4 are utilized for the buck/boost and inverter operation.

Additional switches Q_5 and Q_9 are used only in the inverter

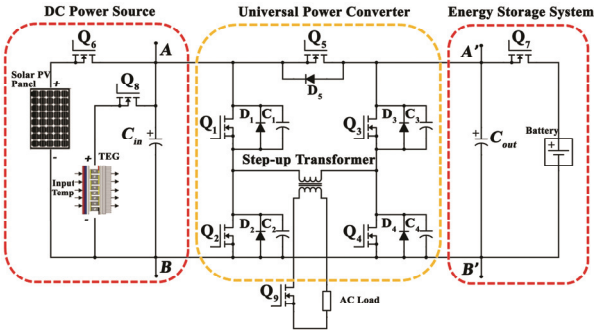

Fig. 1. Circuit diagram of the UPC.

mode to provide an H-bridge configuration for AC power generation. A 12-V/230-V AC step-up transformer is used in this converter for boosting the AC voltage at the secondary level. Primary winding acts as a buck/boost inductor during DC power conversion. Converter circuit components are designed and selected from an experimental study of input power sources. The availability of energy in the sources determines three modes of operation.

A. Modes of Operation of UPC

Buck, boost, and inverter modes of operation with eight important cases are considered for mode selection as follows.

Mode-1: The buck mode of the UPC has two different cases of energy harvesting from a DC source to an energy storage system (i.e., Li-ion battery). This mode is selected for recharging the battery when the battery voltage (V_{BAT}) < 9 V.

Case 1: If a solar panel output voltage (V_{PV}) > 12 V and the TEG's output voltage (V_{TEG}) < 12 V, then switch Q_6 is turned-*ON*, as shown in Fig. 2(a). Switches Q_3 and Q_7 are continuously *ON* in this case to transfer regulated DC power from the converter to the battery. The unregulated DC power from the solar panel is regulated by controlling the pulse-modulated input to MOSFET switch Q_1 using the modified stepped perturb and observe (MSPO) algorithm.

Case 2: If the TEG output voltage (V_{TEG}) >12 V and the solar panel output voltage (V_{PV}) <12 V, then switch Q_8 is turned-*ON*. The switching operation, as mentioned in Case 1, is performed to store TEG power in the battery, as illustrated in Fig. 2.

When Q_1 is ON and D_2 is OFF,

$$\begin{cases} \dfrac{dV_{o1}}{dT_{on}} = \dfrac{(I_{Lp1} - I_{o1})}{C_{out}} \\ \dfrac{dI_{Lp1}}{dT_{on}} = \dfrac{(V_{in} - V_{o1})}{L_p} \end{cases} \quad (1)$$

when Q_1 is OFF and D_2 is ON,

$$\begin{cases} \dfrac{dV_{o1}}{dT_{off}} = \dfrac{(I_{Lp1} - I_{o1})}{C_{out}} \\ \dfrac{dI_{Lp1}}{dT_{off}} = \dfrac{-V_{o1}}{L_p} \end{cases} \quad (2)$$

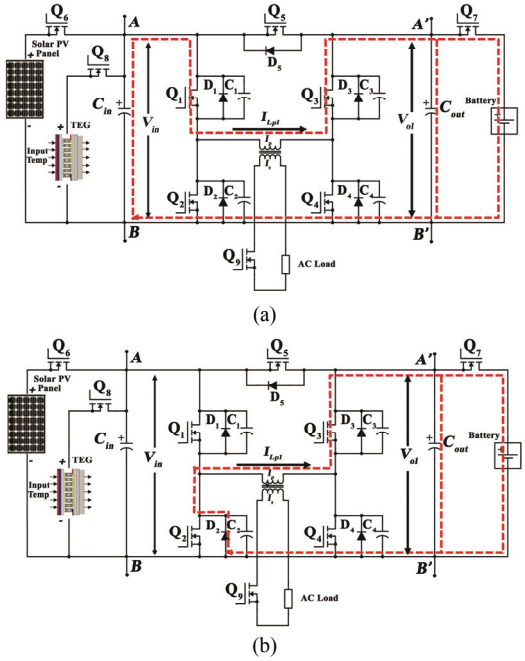

(a)

(b)

Fig. 2. Equivalent circuit of the UPC in buck mode using SPV/TEG power: (a) Power switch Q_1 is *ON* for *0–t1* time interval; (b) Power switch Q_1 is *OFF* for t_1–t_2 time interval.

where

V_{in} - input source voltage (i.e., V_{PV} or V_{TEG}) (V),
V_{o1} - buck mode output voltage (V),
I_{o1} - charging current to battery (A),
I_{Lp1} - Mode-1 current through inductor L_p (A),
L_p - primary winding inductance of transformer (μH),
C_{out} - output filter capacitance (μF).

In steady-state analysis, a continuous conduction mode (CCM) of operation in the buck mode of the UPC is considered and illustrated in Fig. 3. The relationship between the output voltage (V_{o1}), current through inductor L_p, and duty cycle D of the converter is given as follows.

When Q_1 is ON and D_2 is OFF for a period (*0 - t1*),

$$\begin{cases} V_{Lp1(on)} = V_{in} - V_{o1} \\ I_{Lp1\,(on)} = \dfrac{(V_{in} - V_{o1})}{L_p}\ T_{on} = I_{Q1} \end{cases} \quad (3)$$

When Q_1 is OFF and D_2 is ON for a period ($t_1 - t_2$),

$$\begin{cases} V_{Lp1(off)} = -V_{o1} \\ I_{Lp1(off)} = \dfrac{-V_{o1}}{L_p}\ T_{off} = I_{D1} \end{cases} \quad (4)$$

The turn-on and turn-off periods of the switch can be expressed as follows:

$$\begin{cases} T_{on} = DT \\ T_{off} = (1-D)T \end{cases} \quad (5)$$

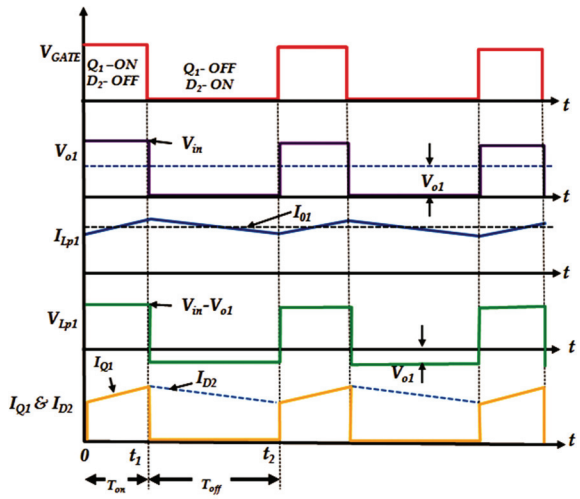

Fig. 3. Switching characteristics of the UPC in buck mode.

The total period is

$$T=T_{on}+T_{off}=\frac{1}{f_s}, \tag{6}$$

where

T_{on} - turn-on period of switch Q_1 (μs),
T_{off} - turn-off period of switch Q_1 (μs),
D - duty cycle of the converter,
f_s - switching frequency of converter (kHz).

In the steady state analysis, the average voltage across the inductor is zero and expressed as follows:

$$(V_{in}- V_{o1})DT= V_{o1}(1-D)T. \tag{7}$$

In the buck operating mode shown in Fig. 2, the output voltage in buck mode is always less than that of the input DC link voltage (V_{in}).

$$V_{o1}=V_{in}\,D \tag{8}$$

Hence, the *ON* and *OFF* time-periods of switch Q_1 is controlled by the MSPO-based duty cycle (Equation 24) control unit. At T_{on} (i.e., *0–t1*) or DT, switch Q_1 is *ON* and the voltage from a DC source appears across an inductor (i.e., primary winding of transformer L_p). A gate pulse to switch Q_1 is stopped when a current through an inductor reaches its maximum level or the turn-on period (T_{on}) estimated by a duty cycle controller reaches its limit. The average value of inductor current is equal to output current I_{o1} and expressed as

$$I_{o1}=\frac{(I_{Lp1(min)}+ I_{Lp1(max)})}{2}, \tag{9}$$

where

$$\begin{cases} I_{Lp1(min)}=I_{o1} - \dfrac{(V_{in}-V_{o1})}{2L_p}DT \\ I_{Lp1(max)}=I_{o1}+\dfrac{(V_{in}-V_{o1})}{2L_p}DT \end{cases} \tag{10}$$

Thus, the current ripples in the inductor can be expressed as

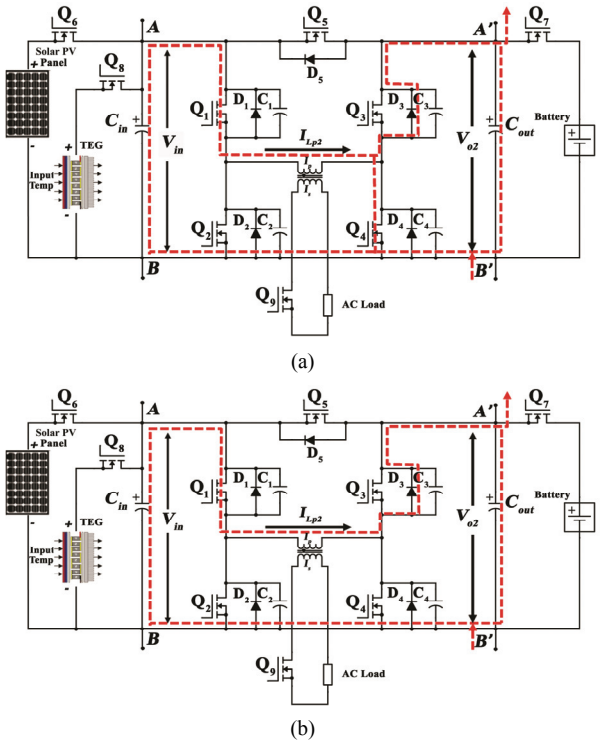

Fig. 4. Equivalent circuit of the UPC in boost mode using SPV/TEG power: (a) Power switch Q_4 is *ON* for *0–t1* time interval; (b) Power switch Q_4 is *OFF* for t_1–t_2 time interval.

$$\Delta I_{Lp1}=I_{Lp1(min)}-I_{Lp1(max)}=\frac{(V_{in}-V_{o1})}{L_p}DT. \tag{11}$$

Once a gate signal is turned-*OFF* at the t_1–t_2 time duration, as indicated in Fig. 3, the energy stored in the inductor is transferred to the load through diode D_2.

Mode-2: Boost mode is chosen when the voltage of a battery (V_{BAT}) ≥12 V. The DC output voltage from this mode is set to 24 V. The converted output may be used to power direct DC loads or connected to an external inverter circuit for connecting AC loads.

Case 3: If the solar panel output voltage (V_{PV}) > TEG output voltage (V_{TEG}) and battery output voltage (V_{BAT}), then switch Q_6 is turned-*ON* to connect the SPV voltage to the converter, as shown in Fig. 4(a). Switch Q_4 is controlled using the MSPO algorithm to provide a suitable duty cycle to obtain the required output voltage from the converter. In this case, switch Q_1 remains *ON* for the entire operation, and switches Q_6 and Q_7 are turned-*OFF* to receive a higher output voltage at terminals A'B'.

Case 4: When the TEG output voltage (V_{TEG}) > solar panel output voltage (V_{PV}) and battery output voltage (V_{BAT}), then switch Q_8 is turned-*ON* to deliver a TEG voltage to the UPC. The control of converter switches, as stated in Case 3, remains the same as in Fig. 4.

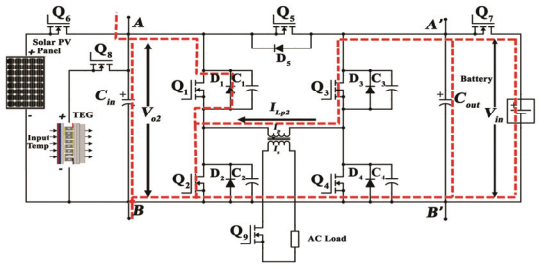

(a)

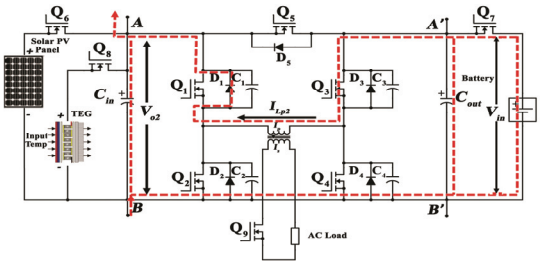

(b)

Fig. 5. Equivalent circuit of the UPC in boost mode using battery power: (a) Power switch Q_2 is *ON* for 0–t_1 time interval; (b) Power switch Q_2 is *OFF* for t_1–t_2 time interval.

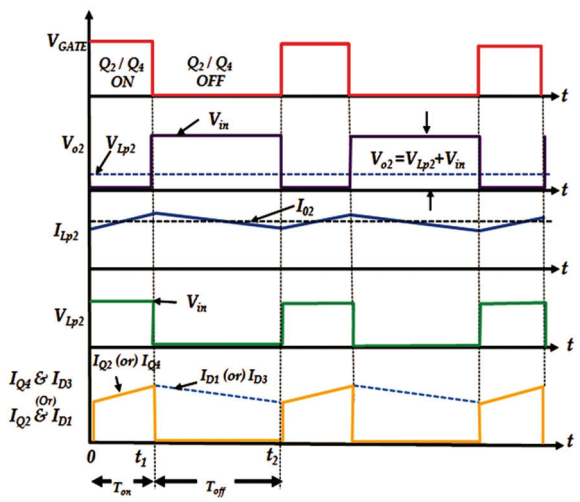

Fig. 6. Switching characteristics of the UPC in boost mode.

Case 5: If the battery output voltage (V_{BAT}) > solar panel output voltage (V_{PV}) and TEG output voltage (V_{TEG}), then switch Q_7 is turned-*ON* to utilize the battery power for boost-up operation, as shown in Fig. 5. In this mode, the converted output voltage is received at terminals *AB*.

During Q_2/Q_4 is ON and D_1/D_3 is OFF

$$\begin{cases} \dfrac{dV_{o2}}{dT_{on}} = \dfrac{I_{o2}}{C_{out}} \\ \dfrac{dI_{Lp2}}{dT_{on}} = \dfrac{V_{in}}{L_p} \end{cases} \tag{12}$$

During Q_2/Q_4 is OFF and D_1/D_3 is ON

$$\begin{cases} \dfrac{dV_{o2}}{dT_{off}} = \dfrac{(I_{Lp2}- I_{o2})}{C_{out}} \\ \dfrac{dI_{Lp2}}{dT_{off}} = \dfrac{(V_{in}-V_{o2})}{L_p} \end{cases} \tag{13}$$

In Fig. 6, the minimum value of inductance for the CCM in boost mode operation is calculated using the inductor current equation.

When Q_2/Q_4 is ON and D_1/D_3 is OFF for a period, $(0 - t_1)$

$$\begin{aligned} V_{Lp2(on)} &= V_{in} \\ I_{Lp2(on)} &= \frac{V_{in}}{L_{p1}}\, T_{on} \end{aligned} \tag{14}$$

When Q_2/Q_4 is OFF and D_1/D_3 is ON for a period $(t_1–t_2)$,

$$\begin{cases} V_{Lp2(off)} = V_{in}- V_{o2} \\ I_{Lp2(off)} = \dfrac{(V_{in}-V_{o2})}{L_{p1}}\, T_{off} \end{cases} \tag{15}$$

The average value of voltage across the inductor in boost mode is zero. Thus, the steady state equation becomes

$$V_{in}\, DT = (V_{in}- V_{o2})(1-D)T. \tag{16}$$

The output voltage of the converter is the sum of the inductor voltage during switch turn-on period and the source voltage during turn-off period.

$$V_{o2} = \frac{V_{in}}{(1-D)} \tag{17}$$

The output voltage (V_{o2}) of the converter in boost mode is higher than the input voltage. The average value of the inductor current is equal to the output current (I_{o2}) and expressed as

$$I_{o2} = \frac{(I_{Lp2(min)}+I_{Lp2(max)})}{2}, \tag{18}$$

where

$$\begin{cases} I_{Lp2(min)} = \dfrac{I_{o2}}{(1-D)} - \dfrac{V_{in}}{2L_p}\, DT \\ I_{Lp2(max)} = \dfrac{I_{o2}}{(1-D)} + \dfrac{V_{in}}{2L_p}\, DT \end{cases} \tag{19}$$

Thus, the current ripple in the inductor can be expressed as

$$\Delta I_{Lp2} = I_{Lp2(min)} - I_{Lp2(max)} = \frac{V_{in}}{L_p}\, DT. \tag{20}$$

The design of circuit elements, such as inductor, capacitor, and switching devices, are discussed in Section III.

Mode-3: A source selection in the inverter mode of UPC is performed similar to the buck/boost mode of operation, and gate pulses to inverter switches Q_1, Q_2, Q_3 and Q_4 are applied using sinusoidal PWM (SPWM). Switches Q_5 and Q_9 are switched on for the entire inverter mode of operation.

Case 6: If solar panel output voltage (V_{PV}) > TEG output voltage (V_{TEG}) and battery output voltage (V_{BAT}), then switch Q_6 is turned-*ON* to connect the SPV voltage to the converter, as shown in Fig. 7(a).

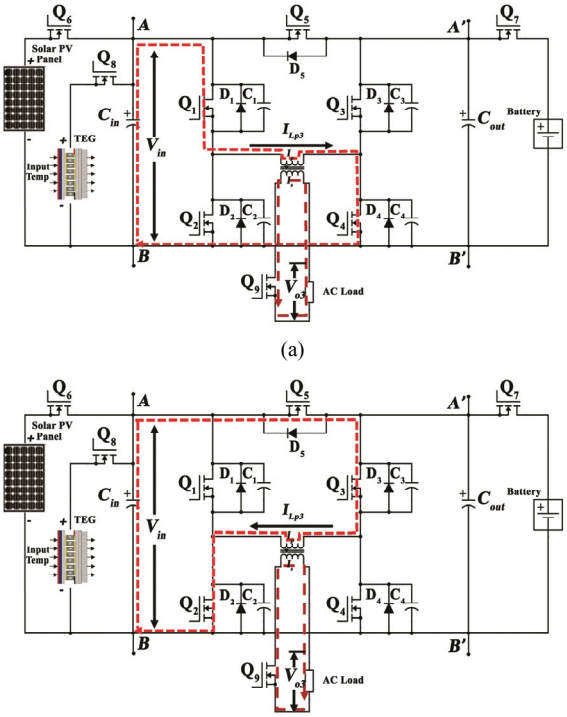

(a)

(b)

Fig. 7. Equivalent circuit of the UPC in inverter mode using SPV/TEG power: (a) Power switches Q_1 and Q_4 are *ON* for 0–t_1 time interval; (b) Power switches Q_2 and Q_3 are *ON* for t_1–t_2 time interval.

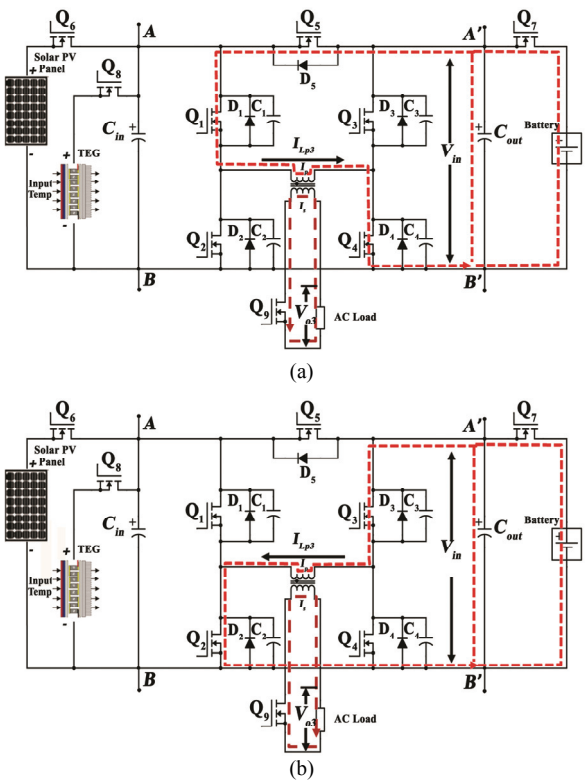

(a)

(b)

Fig. 8. Equivalent circuit of the UPC in inverter mode using battery power: (a) Power switches Q_1 and Q_4 are *ON* for 0–t_1 time interval; (b) Power switches Q_2 and Q_3 are *ON* for t_1–t_2 time interval.

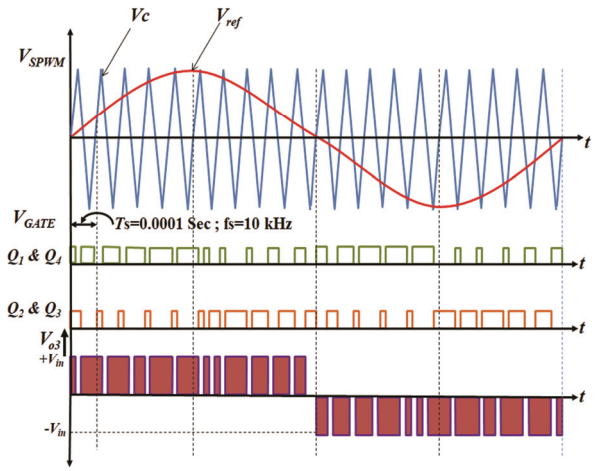

Fig. 9. Gate signal generation using SPWM.

Switches Q_1–Q_4 are controlled using SPWM to generate low voltage AC output from the converter. The low voltage AC generated can be converted into high voltage AC using a step-up transformer. Switch Q_9 is used for connecting the AC load to an inverter, and switch Q_5 is utilized to maintain the symmetry of the H-bridge inverter connection.

Case 7: If TEG output voltage (V_{TEG}) > solar panel output voltage (V_{PV}) and battery output voltage (V_{BAT}), then switch Q_8 is turned-*ON* to deliver TEG voltage to the UPC as illustrated in Fig. 7. The control of converter switches, as stated in Case 6, is followed to obtain a high AC voltage from the converter.

Case 8: If battery output voltage (V_{BAT}) > solar panel output voltage (V_{PV}) and TEG output voltage (V_{TEG}), then switch Q_7 is turned-*ON* to utilize the battery power for DC–AC power conversion. The power flow from the battery to the AC load is presented in Fig. 8.

Switches Q_1Q_4 and Q_2Q_3 are turned-*ON* and *OFF*, respectively. In (0–t_1) duration, switches Q_1Q_4 is ON and Q_2Q_3 is OFF. Then, the input voltage will appear across inductor L_p. If switches Q_1Q_4 are turned-*OFF* and Q_2Q_3 are turned-*ON* from t_1–t_2, the voltage across inductor L_p is reversed.

The square wave output voltage of the UPC in inverter mode is expressed as follows:

$$V_{o3} = \sum_{n=1}^{\infty} V_m \sin(n\omega t). \tag{21}$$

The magnitude of the output voltage (V_m) is obtained as

$$V_m = \frac{1}{\pi}\left[\int_0^{\frac{\pi}{2}} \frac{V_{in}}{2} d(\omega t) + \int_{\frac{\pi}{2}}^{\frac{-\pi}{2}} \frac{-V_{in}}{2} d(\omega t)\right] = \frac{4V_{in}}{n\pi}. \tag{22}$$

Thus, the output voltage of the converter can be denoted as

$$V_{o3} = \sum_{n=1}^{\infty} \frac{4V_{in}}{n\pi} \sin(n\omega t). \tag{23}$$

The output voltage (V_{o3}) and the corresponding gate pulses for the inverter mode are illustrated in Fig. 9.

TABLE I
SPECIFICATION OF SPV PANEL AND TEG

Parameters	Value
Poly-Crystalline - Solar PV Panel	
V_{mp}: Optimum Operating Voltage	17.2 V
I_{mp}: Optimum Operating Current	5.81 A
V_{oc}: Open-Circuit Voltage	21.6 V
I_{sc}: Short-Circuit Current	6.52 A
N_c: No. of Cells	4*9 (36)
TEG Module	
V_{max}: Max. Operating Voltage	16.4 V
I_{max}: Max. Operating Current	8.4 A
R_m: Module Resistance	2.3 Ohms
T_H: Hot Side Temperature	50 °C
T_{max}: Delta Max	75 °C

B. Design Specification of UPC

The specifications of the SPV panel and the TEG module are presented in Table I. The V–I characteristics of the SPV panel are obtained for various irradiation and temperature inputs. Similarly, the TEG module is tested for various temperature inputs, and the experimental data are presented in Table II. The minimum and maximum changes in output voltages and currents from these sources are considered for the design and selection of UPC circuit elements.

The nominal switching frequency of the converter is considered as f_{sw}=10 kHz. In buck mode, the nominal charging voltage required by a 12-V battery is 13.5 V, which is less than the input source voltage magnitude (i.e., V_{in}= 16.3 V). Hence, the duty cycle of the converter is calculated using Equation (24).

$$D_{Buck}=\left(\frac{V_o}{V_{in}}\right) \tag{24}$$

Hence, the maximum duty cycle of *0.84* is estimated for buck mode. Similarly, in boost mode the minimum and maximum values of the duty cycle are determined using Equations (25)–(26) to maintain an output voltage of 24 V.

$$D_{(min)}=1-\left(\frac{V_{in\,(max)}}{V_0}\right) \tag{25}$$

$$D_{(max)}=1-\left(\frac{V_{in\,(min)}}{V_o}\right) \tag{26}$$

In boost mode, $V_{in(min)}$ = 14.4 V and $V_{in(max)}$ = 16.3 V, which are obtained from the experimental data shown in Table II. Hence, to achieve a constant 24-V DC voltage in boost mode, the duty cycle is varied from $D_{(min)}$= 0.32 to $D_{(max)}$ = 0.4.

Inductor Design: The values of the inductor used in the UPC's buck and boost modes of operation are calculated separately.

$$L_{Buck}>\frac{V_o(V_{in}-V_o)}{\Delta I_{Lp1}*f_{sw}*V_{in}} \tag{27}$$

$$L_{Boost}>\frac{D*V_{in}*(1-D)}{(2*f_{sw}*I_{o2})} \tag{28}$$

From Equations (27) and (28), the inductance values are obtained as L_{Buck} = 231.9 μH and L_{Boost} = 39.12 μH. However, the proposed converter requires a single inductor for both buck and boost modes of operation. Hence, the primary step-up transformer is selected based on the highest value of inductor requirement, which is L = 231.9 μH. The same is used in the inverter operation.

This inductor selection may result in the increase/decrease of the output voltage magnitude during boost operation. Therefore, the maximum duty cycle of the boost operation is changed to $D_{(max)}$ = 0.42 with respect to the maximum inductance from Equation (28).

$$I_{peak}=\frac{V_{in(max)}*D}{f_{sw}*L} \tag{29}$$

The peak value of the inductor current can be determined to select the proper inductor value.

TABLE II
EXPERIMENTAL DATA OF SOLAR PV & TEG MODULE

Solar Panel				*TEG Module*			
Temperature (°C)	Irradiation (W/m^2)	Voltage (V)	Current (A)	Hot Side Temperature (°C)	Cold Side Temperature (°C)	Voltage (V)	Current (A)
26.3	250	14.9	3.8	60	25	14.4	5.2
27.2	520	15.8	4.2	65	28	14.9	6.1
28.6	630	16.0	5.6	66	32	15.1	6.5
28.9	640	16.1	5.8	70	35	15.4	6.9
29.0	650	16.3	5.8	75	36	15.6	7.2
29.8	570	15.4	6.7	76	36	15.6	7.2
30.2	480	15.2	7.1	78	38	15.8	7.8
31.6	310	14.9	7.5	80	37	16.2	7.8

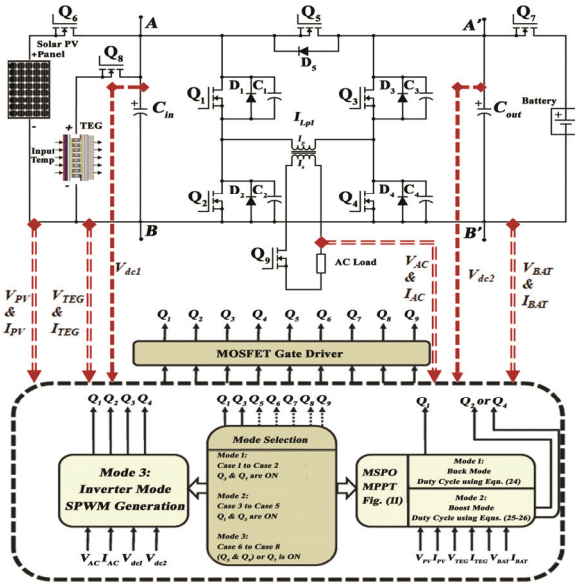

Fig. 10. Control Structure of the UPC using dsPIC30F4011.

Capacitor Design: The minimum value of the input capacitor is necessary for stabilizing the input voltage due to the peak current requirement of a switching power supply. The capacitor value can be increased if the input voltage has a high ripple content. Equation (30) can be used to adjust the output capacitor values to obtain the desired output voltage with a ripple of 0.5 V:

$$C_{out} > \frac{I_{o1}}{V_{ripple} * f_{sw}}. \tag{30}$$

The minimum output capacitance value required is C_{out} = 1000 µF. The actual value of capacitance selected is higher than the critical capacitance of the boost converter.

III. UPC Control Structure

The proposed system is controlled using a dsPIC30F4011 digital controller. The controller monitors the voltage and current delivered by the power sources, namely, SPV, TEG, and battery. The operating modes are selected based on the source voltage magnitudes. The overall control architecture is illustrated in Fig. 10. Modes 1 and 2 use the MSPO algorithm for the duty cycle generation to the converter switches. In Mode 3, the inverter mode of operation SPWM strategy is used for AC voltage generation.

A. Modified Stepped Perturb and Observe (MSPO)

Perturbation and observation (P&O) is an efficient maximum power point tracking (MPPT) strategy. In general, the P&O algorithm uses a fixed step size, which is determined by the accuracy and tracking speed requirements. However, if the step size is increased for tracking speed-up, the accuracy is decreased.

This condition is due to the failure of P&O to track power under rapidly varying atmospheric conditions, resulting in a comparatively low efficiency, and vice versa. These drawbacks of the traditional P&O algorithm can be eliminated by varying the step size under rapidly varying atmospheric conditions.

In this work, a modified stepped P&O (MSPO) algorithm is proposed for MPPT and is dedicated to finding a simple but effective means improving tracking accuracy and overcoming the drawbacks in traditional MPPT algorithms. The MSPO algorithm is designed to effectively reduce power losses in systems and operate DC power sources at the maximum operating point. The flow of the MSPO-MPPT algorithm is depicted in Fig. 11 where the step size is automatically tuned according to the DC source operating point. If the operating point is far from the MPP, then the step size is increased, thereby enabling fast-tracking capability. The proposed MPPT controller thus changes the duty ratio of the buck/boost converter as follows:

$$D^*(k) = D(k) - \frac{\Delta P}{\Delta I}, \tag{31}$$

where ΔP is the change in output power in watts and ΔI is the change in load current in amps. The MPPT control system has an inherent characteristic in three criteria.

(i) $\frac{\Delta P}{\Delta I} > 0$ DC source operating point at left of MPP

(ii) $\frac{\Delta P}{\Delta I} = 0$ DC source operating point at MPP

(iii) $\frac{\Delta P}{\Delta I} < 0$ DC source operating point at right of MPP

B. Sinusoidal Pulse Width Modulation (SPWM)

The most widely used method of PWM is carrier-based. A sinusoidal modulation is based on a triangular carrier signal, and the level comparison between them produces the PWM gating signal, as shown in Fig. 9. In this work, SPWM is implemented using a dsPIC30F4011 microcontroller. In Mode 3, the output AC voltage frequency is set to be 50 Hz and has a period of 20 ms (one full cycle). The half-cycle period of 10 ms is utilized to generate the positive and negative cycles of the sine wave. The pulses are varied according to the amplitude of the sine wave. However, the total time of all pulses should be equal to 10 ms. In this work, the switching frequency (f_s) is 10 kHz. Hence, the period of each pulse is equal to 100 µs, and the number of pulses is

$$\textit{Number of Pulses in SPWM} = \left[\frac{\textit{Time Period of Half Cycle of Sine Wave}}{\left(\frac{1}{f_s}\right)} \right]. \tag{32}$$

From Equation (32), the number of pulses is derived as (10 ms / 100 µs =100 pulses). The relationship of the sine wave with its phase angle and peak value is given as follows:

$$X = A * \text{sine (Angle)} \tag{33}$$

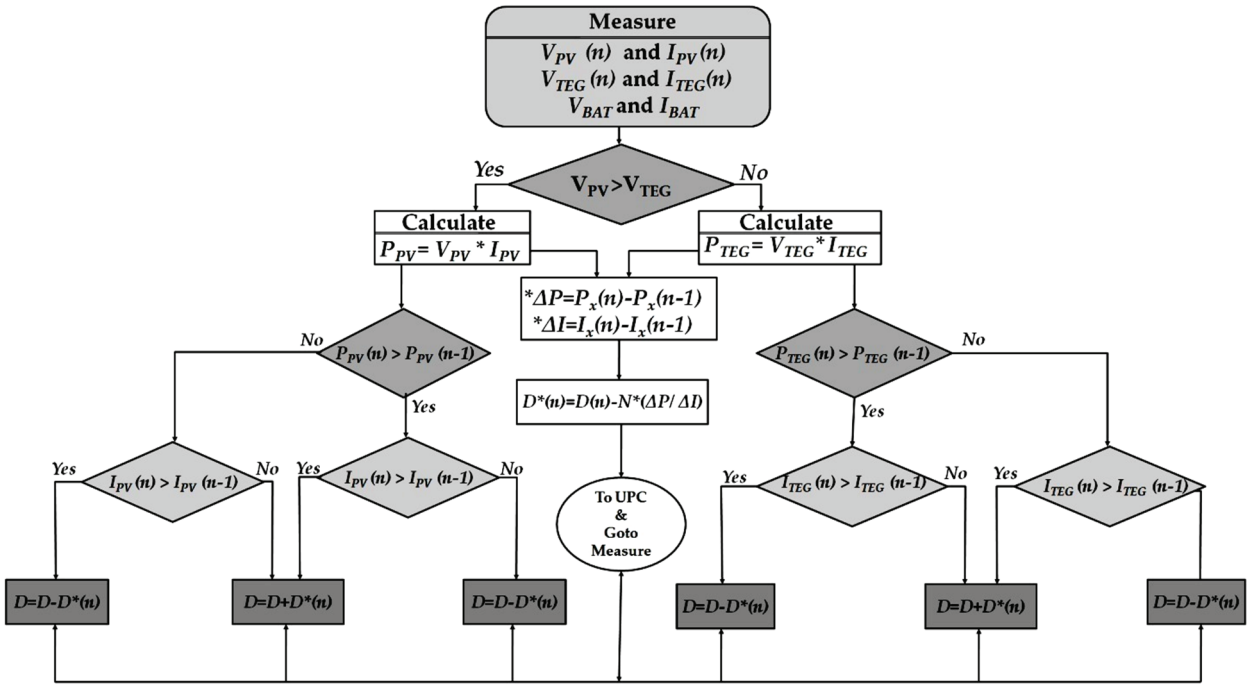

Fig. 11. Flowchart of the MSPO algorithm.

TABLE III
DATA FOR SINE WAVE GENERATION USING DSPIC30F4011

Interval	Angle in degree	Value X = Sine(Angle)	Duty Cycle Y = X*250
1	18	0.3090	77.2
2	36	0.5877	146.9
3	54	0.8090	202.2
4	72	0.9511	237.7
5	90	1	250
6	90	1	250
7	72	0.9511	237.7
8	54	0.8090	202.2
9	36	0.5877	146.9
10	18	0.3090	77.2

where the half-cycle of the sine wave consists of 180 degrees, which are then divided into 10 equal parts. Hence, the value of each pulse step is 180/10 = 18 degrees. The values found for the 10 equal intervals are presented in Table III, and these values are converted into duty cycle by multiplying them with the maximum duty cycle value, which is generated by the microcontroller.

In dsPIC30F4011, a duty cycle changes from 0 to 255 (where 0 means 0% duty cycle and 255 means 100% duty cycle). Hence, the highest value of 255 is multiplied with the sine angle, and the duty cycles of the pulses are obtained and presented in Table II.

The phase legs of the inverter must be protected from short circuit. Therefore, an appropriate delay time in the controller is introduced between the gating signals in the designed SPWM architecture. Meanwhile, the highest value of 255 is reduced to 250, and 5 is allocated as the delay time for the signals. Thus, the duty cycle or width of each pulse is {77.2, 146.9, 202.2, 237.7, 250, 250, 237.7, 202.2, 146.9, and 77.2}. These pulses are used to control switches Q_1 to Q_4 in the UPC.

IV. RESULTS AND DISCUSSION

The hardware arrangement of the UPC is shown in Fig. 12. The converter operates at 10 kHz switching frequency. Nine MOSFET switches and five diodes are used for the UPC configuration. The MOSFET switches and diodes are IRF540 and 10A02, respectively. The controller is implemented using the microchip dsPIC30F4011 microcontroller.

A. Buck Mode of Operation

The prototype model of the proposed system is observed in buck mode with the MSPO algorithm. The performance of the controller is evaluated with PV/TEG input values of 14.8 V/16 V.

The output voltage is obtained from the buck mode as 14.6 V. The output obtained with 16 V reference value is illustrated in Fig. 13. The output voltage ripple is remarkably small (0.08 V), and the output voltage settles down rapidly. The duty cycle calculation from the hardware occurs instantaneously as per the MSPO algorithm, as shown in Fig. 11.

The buck mode simulation result is presented in Fig. 14, which shows a 3.278 A charging current from the buck converter and 0.03 A inductor current ripple.

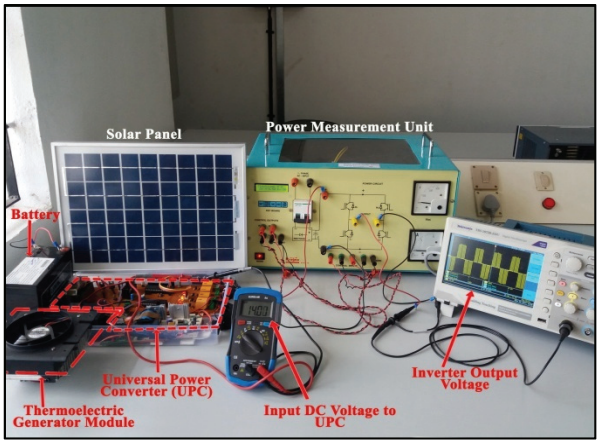

Fig. 12. Hardware structure of the UPC.

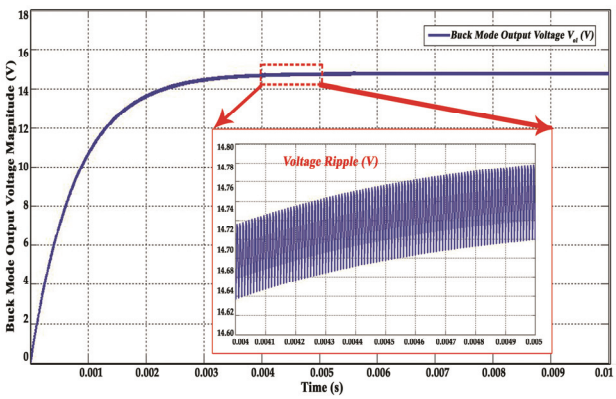

Fig. 13. Buck converter output voltage magnitude with ripple.

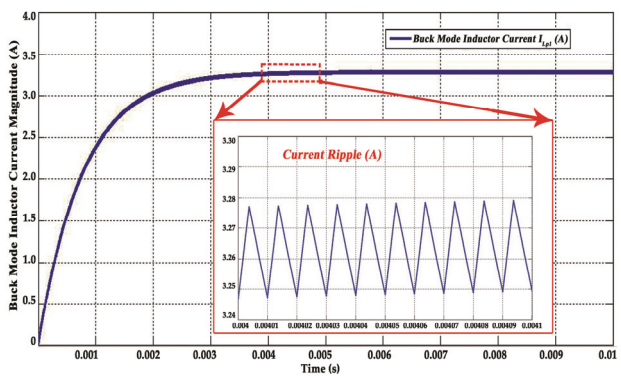

Fig. 14. Buck converter inductor current magnitude with ripple.

The experimental result of the buck mode is presented in Fig. 15. The PWM pulses are generated from the dsPIC30F4011 controller within a short duration of time without any delay or time lag. The experimental results obtained are thus consistent with the simulation results and mathematical calculations.

The charging current from the buck converter is 3.32 A, and the inductor current ripple value is monitored in the converter, which has the value of 0.05 A in the output. The initial duty cycle of the converter is 0.84, which varies randomly with respect to the input voltage change.

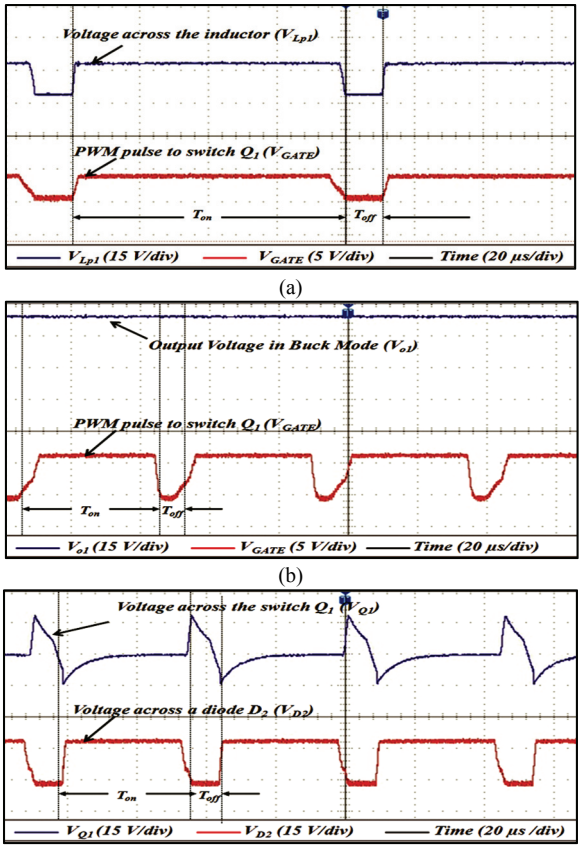

Fig. 15. Experimental results for the UPC in buck mode.

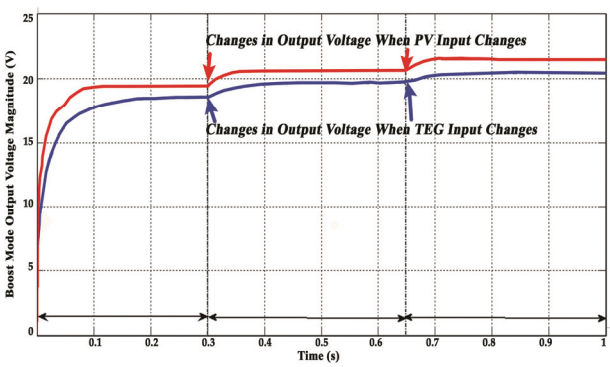

Fig. 16. Boost converter output voltage magnitude.

B. *Boost Mode of Operation*

The output voltages of the boost mode of operation are measured for the SPV panel and the TEG inputs. The same MSPO algorithm is used to track the maximum operating point of a DC input. The simulation results of the boost mode are presented in Fig. 16, which shows the variation in the generated output voltages from the SPV panel and the TEG. These sources have a voltage variation of approximately 14 V to 18 V under varying climate conditions, such as temperature and irradiation conditions.

The experimental result of the boost mode is presented in Fig. 17. The duty cycle of the UPC in boost mode is varied

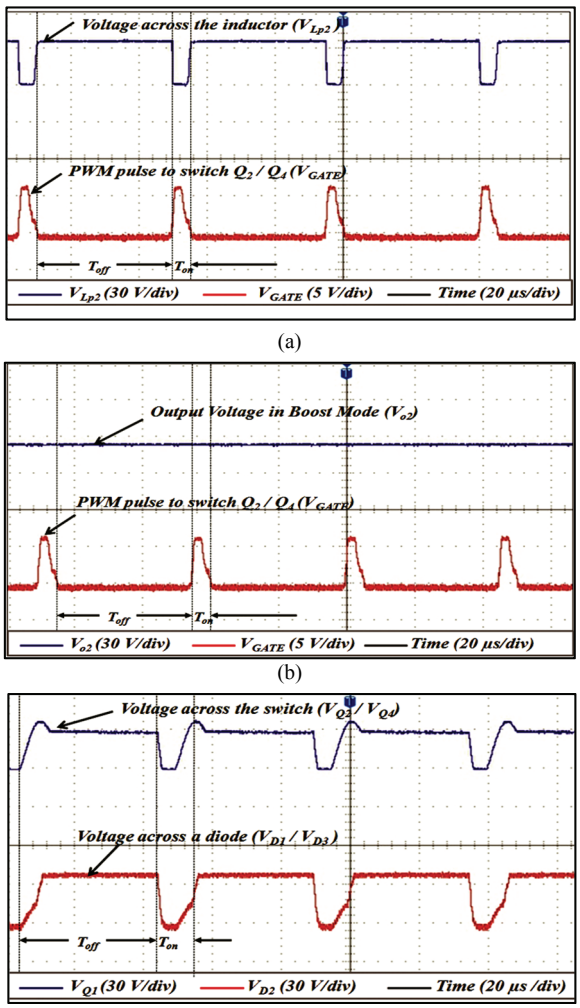

Fig. 17. Experimental results for the UPC in boost mode.

from 0.36 to 0.42 using the dsPIC30F4011 microcontroller.

The output voltage ripple is also small (0.5 V). The results obtained clearly show that the boost converter steps up the voltage from 9 V/16.4 V to 24 V in accordance with the parameters derived from Equations (24) to (30), hence fulfilling the desired conditions of the output current, that is, 7.8 A at a frequency of 10 kHz. The efficiency of the boost converter is 96.2% under full load condition.

C. Inverter Mode of Operation

The inverter mode of operation in the UPC is analyzed at the same switching frequency (10 kHz). The modulation index (M) of the SPWM pulse is varied from 0.3 to 0.9. The 12 V output voltage from the inverter mode is stepped up using a step-up transformer.

Fig. 18 shows the output AC voltage magnitude and the total harmonic distortion (THD) spectrum. When the modulation index M = 0.3, the AC voltage magnitude is 192.8 V and has higher-order frequencies in the output. The percentage THD is 6.19%, which is reduced by adjusting the modulation index.

In Fig. 19, the modulation index is increased from M = 0.9,

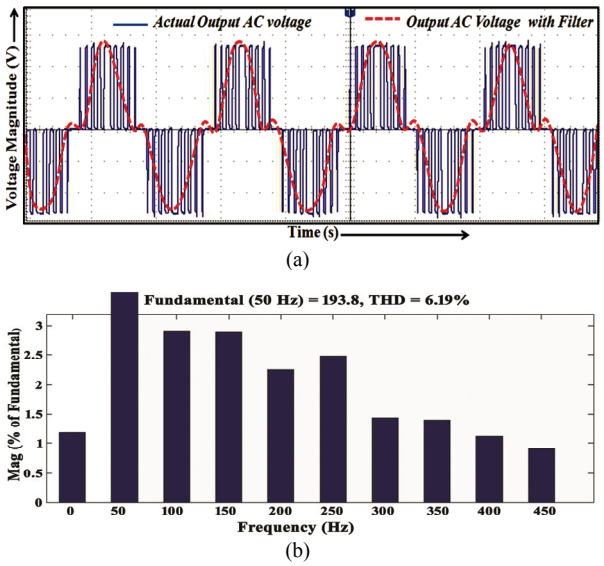

Fig. 18. Inverter output at SPWM modulation index M=0.3: (a) Output voltage magnitude; (b) THD spectrum.

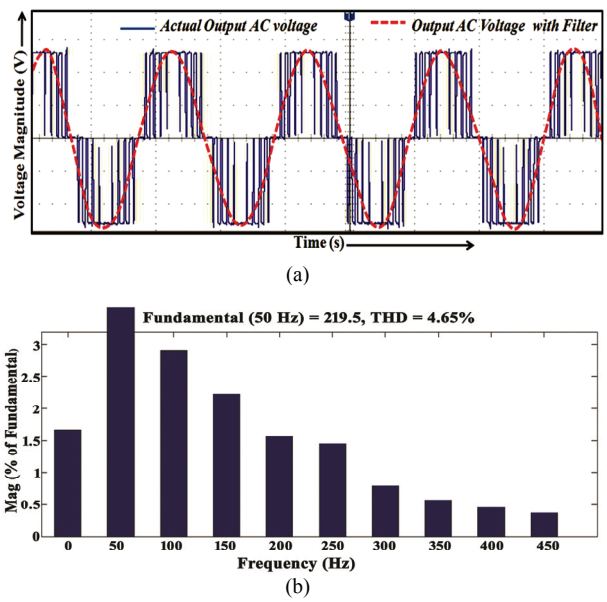

Fig. 19. Inverter output at SPWM modulation index M = 0.9: (a) Output voltage magnitude; (b) THD spectrum.

and the AC voltage magnitude is 219.5 V, with a THD of 4.65%, which is at the standard level. The efficiency of the UPC in the inverter mode is 97%, including the switching losses.

Comparative analysis is performed with the literature study, and the performance of the converter in buck, boost, and inverter modes of operation is presented in Table IV. The proposed converter and its PWM control methods are effective in regulating the output power and operating the converter at the highest efficiency of 97%.

D. Calculation of UPC Efficiency

The efficiency of the converter is estimated in individual

TABLE IV
PERFORMANCE EVALUATION

Design Parameters	Buck Mode			Boost Mode			Inverter Mode		
	[2]	[5]	Proposed UPC	[22]	[11]	Proposed UPC	[14]	[17]	Proposed UPC
Year	2016	2016		2018	2017		2016	2013	
V_{in} (V)	3.0–3.6	25	14.8–16	200	265	9–16.4	185	380	9–12
V_o (V)	1.0–1.8	12	14–14.6	350	400	24	200	240	220
Control Mechanism	PLASOM	DBV	MSPO PWM	PWM	PWM	MSPO PWM	3LD-PWM	SPWM	SPWM
Filter Capacitor (μF)	10	220	1000	360	680	1000	N.A.	2.2	N.A.
Inductor (μH)	4.7	4.7	231.9	70×10^3	81	231.9	N.A.	N.A.	N.A.
Switching Frequency (kHz)	100	1800	10	100	50	10	10	20	10
Load Current I_o (A)	0.5	5	3.32	2.8	1.25	7.8	4	21	0.8
Output Voltage Ripple (V)	24×10^{-3}	N.A.	0.5	N.A.	7.35	1.8	N.A.		
Power Loss (W)	23×10^{-3}	7.2	1.29	21.2	66.8	4.71	2.65	50	4.69
Full Load Efficiency η (%)	96.2	88	97.4	98.8	97.4	96.2	93.1	99	97.4

modes. The losses in the converter elements, such as inductor, diode, and MOSFET, are considered in the efficiency calculation. The inductor losses are determined using Equation (34).

$$P_L = I_o^2 * R_{LDC} \ , \tag{34}$$

where I_o is the buck mode current and R_{LDC} is the DC resistance of the inductor, which is 0.093 Ohm.

The power losses in MOSFET switch P_{MOSFET} are obtained from Equations (35) to (37). The turn-on gate pulses to the MOSFET switch increase the current from zero to the final value before the voltage falls from the cut-off voltage to the forward voltage. The maximum switching frequency (f_{Sw}) of the MOSFET is 10 kHz. If a linear current rise-up is assumed, then the average turn-on power losses are approximately

$$P_{MOSFET}(on) \approx \frac{1}{10} * V_{sw} * I_o * \ f_{sw} * t_r \tag{35}$$

where V_{sw} is the voltage across the MOSFET switch, I_o is the load current or current through the switch, and the turn-on current rise time (t_r) of the switch is obtained as 45 ns from a datasheet. Similarly, the turn-off power losses for a MOSFET can be calculated with the fall time (t_f) of 20 ns for the current from the maximum value to zero as follows:

$$P_{MOSFET}(off) \approx \frac{1}{10} * \ V_{sw} * I_o * f_{sw} * t_f \ . \tag{36}$$

The total switching losses of the proposed converter can be determined as

$$P_{MOSFET(Conv)} = n.(P_{MOSFET}(on) + P_{MOSFET}(off) \ ), \tag{37}$$

where n is the number of switches involved in the converter operation.

The total losses in the converter can be obtained from Equation (38), which includes the inductor, MOSFET, and diode power loss P_D.

$$P_T = P_L + P_{MOSFET(Conv)} + P_D \tag{38}$$

The efficiency (η) of the universal power converter is estimated using Equation (39).

$$\eta = \frac{P_0}{P_0 + P_T} * 100\% \tag{39}$$

From the experimental study, the maximum output power of the buck mode of the UPC is 48.47 W. The power loss in the inductor is estimated as 1.025 W using Equation (34). The MOSFET switching losses in buck mode are calculated using Equations (35) and (36) as $P_{MOSFET}(on)$ = 0.2465 mW and $P_{MOSFET}(off)$ = 0.1095 mW, and two MOSFET switches are associated with the buck converter operation. Hence, the total switching loss of the proposed converter in buck mode is 0.7121 mW. The diode has a conduction loss (P_D) of 0.251 W, and the overall loss in the converter is estimated as 1.29 W.

Hence, the efficiency of the converter in buck mode is estimated as 97.4%. Similarly, for the boost converter, the total power delivered (Po) is 187.2 W, and the switching loss of 1.21 W of the two switches and the loss in the diode is estimated as 0.55 W in boost mode. The efficiency in boost mode of operation is 96.2%. In inverter mode, six switches are utilized and only four switches are involved in high-frequency operation. The 0.8 A unity power factor load is connected in the inverter mode of the UPC. The power delivered is 176 W, and the total loss in the converter in inverter mode is approximately 4.69 W. Hence, the efficiency of the converter in inverter mode is predicted as 97.4%, and the average efficiency of the converter is 97%.

V. CONCLUSIONS

A new UPC, which has a highly efficient control strategy in hardware circuit, is designed and analyzed. The buck, boost, and inverter modes of operation are achieved with a small number of converter components, and the results of each modes of operation are clearly presented. The MSPO algorithm is proposed to control the converter in buck and

boost modes to regulate the output voltage for a variable input voltage on the basis of the charge status of the battery supply and the direct DC loads. The control method has improved efficiency and reduces the ripple content of the output voltage in the buck/boost mode of the UPC whenever low transition is needed. The inverter mode is analyzed when the power from the DC sources is higher than 12 V, and SPWM is implemented to obtain a harmonics-free AC output and a THD% of 4.65%, which is maintained as per the IEEE:519 standard. In this control method, the UPC significantly improves the efficiency to 97%. The experimental results validate the proposed UPC and the merits of its control methods. The novel method can be utilized to improve output voltage transients in transition in the buck, boost, and inverter modes of operations.

REFERENCES

[1] The International Energy Agency (IEA), "World Energy Outlook-2017," IEA Publications, pp.1-8, Nov. 2017. https://www.iea.org/Textbase/npsum/weo2017SUM.pdf.

[2] C.-H. Huang and C.-C. Chen, "A high-efficiency current-mode buck converter with a power-loss-aware switch-on-demand modulation technique for multifunction SoCs," *IEEE Trans. Power Electron.,* Vol. 31, No. 12, pp. 8303-8316, Dec. 2016.

[3] D. Vinnikov, A. Chub, R. Kosenko, J. Zakis, and E. Liivik, "Comparison of performance of phase-shift and asymmetrical pulsewidth modulation techniques for the novel galvanically isolated buck–boost DC–DC converter for photovoltaic applications," *IEEE J. Emerg. Sel. Topics Power Electron.*, Vol. 5, No. 2, pp. 624-637, Jun. 2017.

[4] L. Cheng, Y. Liu, and W. H. Ki, "A 10/30 MHz fast reference-tracking buck converter with DDA-based type-III compensator," *IEEE J. Solid-State Circuits*, Vol. 49, No. 12, pp. 2788-2799, Dec. 2014.

[5] W.-C. Chen, Y.-W. Chou, M.-W. Chien, H.-C. Chen, and S.-H. Yang, K.-H. Chen, Y.-H. Lin, C.-C. Lee, S.-R. Lin, and T.-Y. Tsai, "A dynamic bootstrap voltage technique for a high-efficiency buck converter in a universal serial bus power delivery device," *IEEE Trans. Power Electron.*, Vol. 31, No. 4, pp. 3002-3015, Apr. 2016.

[6] A. Rodriguez, A. Vazquez, M. R. Rogina, and F. Briz, "Synchronous boost converter with high efficiency at light load using QSW-ZVS and SiC MOSFETs," *IEEE Trans. Ind. Electron.*, Vol. 65, No. 1, pp. 386-393, Jan. 2018.

[7] B. Honarjoo, S. M. Madani, M. Niroomand, and E. Adib, "Analysis and implementation of a new single switch, high voltage gain DC-DC converter with a wide CCM operation range and reduced components voltage stress," *J. Power Electron.*, Vol. 18, No. 1, pp. 11-22, Jan. 2018.

[8] F. Radmand and A. Jalili, "A novel switched-capacitor based high step-up DC/DC converter for renewable energy system applications," *J. Power Electron.*, Vol. 17, No. 6, pp. 1402-1412, Nov. 2017.

[9] J.-I. Baek, J.-K. Kim, J.-B. Lee, H.-S. Youn, and G.-W. Moon, "A boost PFC stage utilized as half-bridge converter for high-efficiency DC–DC stage in power supply unit," *IEEE Trans. Power Electron.*, Vol. 32, No. 10, pp. 7449-7457, Oct. 2017.

[10] N. ul Hassan, Y.-J. Kim, B.-M. Han, and J.-Y. Lee, "A hybrid DC/DC converter for EV OBCs using full-bridge and resonant converters with a single transformer," *J. Power Electron.,* Vol. 17, No. 1, pp. 11-19, Jan. 2017.

[11] S.-H. Ham, H.-J. Choe, H.-S. Lee, and B. Kang, "Improvement of power-conversion efficiency of AC-DC boost converter using 1:1 transformer," *IEEE Trans. Power Electron.,* Vol. 33, No. 8, pp. 6646-6655, Oct. 2017.

[12] E. M. Ahmed and M. Shoyama, "Variable step size maximum power point tracker using a single variable for stand-alone battery storage PV systems," *J. Power Electron.*, Vol. 11, No. 2, pp. 218-227, Mar. 2011.

[13] G. R. C. Mouli, J. H. Schijffelen, P. Bauer, and M. Zeman, "Design and comparison of a 10-kW interleaved boost converter for PV application using Si and SiC devices," *IEEE J. Emerg. Sel. Topics Power Electron.*, Vol. 5, No. 2, pp. 610-623, Jun. 2017.

[14] A. Harrasi and A. F. Zobaa, "A cost-effective harmonic cancellation method for high-frequency silicon carbide MOSFET-based single phase inverter," *IEEE Power Energy Technol. Syst. J.,* Vol.3, No. 4, pp. 128-142, Dec. 2016.

[15] Y. Levron and R. W. Erickson, "High weighted efficiency in single-phase solar inverters by a variable-frequency peak current controller," *IEEE Trans. Power Electron.*, Vol. 31, No. 1, pp. 248- 257, Jan. 2016.

[16] IEEE Standard 519-2014 Compliances, Updates, Solutions and Case Studies, pp. 1-49, https://www. schneider-electric. com. tw / documents / Event / 2016_electrical_engineering _ seminar/ IEEE_STD_519_1992vs2014.pdf.

[17] B. Ji, J. Wang, and J. Zhao, "High-efficiency single-phase transformerless PV H6 inverter with hybrid modulation method," *IEEE Trans. Ind. Electron.*, Vol. 60, No. 5, pp. 2104-2114, May 2013.

[18] B. Gu, J. Dominic, J.-S. Lai, C.-L. Chen, T. LaBella, and B. Chen, "High reliability and efficiency single-phase transformerless inverter for grid-connected photovoltaic systems," *IEEE Trans. Power Electron.,* Vol. 28, No. 5, pp. 2235-2244, May 2013.

[19] D. Istardi, B. Halim, and A. J. Febriansyah, "High efficiency single phase inverter design," in *Proc. EECSI*, pp. 1-5, 2017.

[20] T. Kerekes, R. Teodorescu, P. Rodríguez, G. Vázquez, and E. Aldabas, "A new high-efficiency single-phase transformerless PV inverter topology," *IEEE Trans. Ind. Electron.*, Vol. 58, No. 1, pp. 184-191, Jan. 2011.

[21] H. Ram´ırez-Murillo, C. Restrepo, T. Konjedic, J. Calvente, A. Romero, C. R. Baier, and R. Giral, "An efficiency comparison of fuel-cell hybrid systems based on the versatile buck–boost converter," *IEEE Trans. Power Electron.*, Vol. 33, No. 2, pp- 1237-1245, Feb. 2018.

[22] H. N. Le and J.-I. Itoh, "Wide-load-range efficiency improvement for high-frequency SiC-based boost converter with hybrid discontinuous current mode," *IEEE Trans. Power Electron.*, Vol. 33, No. 2, pp. 1843-1854, Feb. 2018.

[23] J.-K. Han, J.-W. Kim, and G.-W. Moon, "A high-efficiency asymmetrical half-bridge converter with integrated boost converter in secondary rectifier," *IEEE Trans. Power Electron.*, Vol. 32, No. 11, pp. 8237-8242, Nov. 2017.

[24] X.-E. Hong, J.-F. Wu, and C.-L. Wei, "98.1% efficiency hysteretic-current-mode noninverting buck–boost DC-DC converter with smooth mode transition," *IEEE Trans. Power Electron.*, Vol. 32, No. 3, pp. 2008-2017, Mar. 2017.

[25] M. Amirabadi and S. A. K. H. M. Niapour, "Extremely sparse parallel AC-link universal power converters," *IEEE Trans. Ind. Appl.*, Vol. 52, No. 3, pp. 2456-2466, Feb. 2016.
[26] M. Shousha, D. Dinulovic, and M. Haug, "A universal topology based on buck-boost converter with optimal resistive impedance tracking for energy harvesters in battery powered applications," in *IEEE Conference Proc. APEC,* pp. 2111–2115, May. 2017.
[27] M. Amirabadi, H. A. Toliyat, and J. Baek, "Ultra sparse AC-link converters," *IEEE Trans. Ind. Appl.*, Vol. 51, No. 1, pp. 448-458, Jul. 2015.
[28] M. Amirabadi, "A new class of universal power converters," in *IEEE Conference Proc. ECCE,* pp. 2596-2602, 2015.
[29] M. Amirabadi, "Analog control of the ac link universal power converters: The key to very high frequency AC link conversion systems," in *IEEE Conference Proc. APEC,* pp. 2301-2308, 2015.
[30] K. Mozaffari and M. Amirabadi, "A multifunction series inductive AC-link universal power converter with reduced-switch count," in *IEEE Conference Proc. APEC,* pp. 442-449, 2018.

Sathiyanathan M. received his B.E. in electrical and electronics engineering from Sengunthar Engineering College, Tiruchengode, India, in 2008, and his M.E. in power electronics and drives from PSG College of Technology, Coimbatore, India, in 2012. He is Senior Assistant Professor in the Department of Electrical and Electronics Engineering, PSG Institute of Technology and Applied Research, Coimbatore, India. His research interests include renewable power generation systems and design of DC–DC and DC–AC power converters.

Jaganathan S. received his M.E. in power systems engineering from Government College of Technology, Coimbatore, India, in 2004, and his Ph.D. in electrical engineering from Anna University, Chennai, India, in 2013. He has published over 20 technical papers in reputable international and national journals. He is Professor and Head in the Department of Electrical and Electronics Engineering, Dr. N.G.P. Institute of Technology, Coimbatore, India, and a reviewer of Elsevier, SAGE, and Springer journals. His areas of interest include FACTS controllers, optimization techniques, power electronic converters, and renewable energy systems.

Josephine R. L. received her M.Tech. in power electronics from National Institute of Technology, Tiruchirappalli, India, in 2009, and her Ph.D. in electrical engineering from Coimbatore Institute of Technology, Coimbatore, India. She has published over 15 technical papers in reputed international and national journals. She is Assistant Professor in the Department of Electrical and Electronics Engineering, National Institute of Technology, Tiruchirappalli, India. Her areas of interest include power electronic converters in renewable energy systems.